Int J Comput Vis (2011) 92: 146–161
DOI 10.1007/s11263-009-0311-4

Adaptive Continuous-Scale Morphology for Matrix Fields

Bernhard Burgeth · Luis Pizarro · Michael Breuß · Joachim Weickert

Received: 8 June 2009 / Accepted: 11 November 2009 / Published online: 1 December 2009
© Springer Science+Business Media, LLC 2009

Abstract In this article we consider adaptive, PDE-driven morphological operations for 3D matrix fields arising e.g. in diffusion tensor magnetic resonance imaging (DT-MRI). The anisotropic evolution is steered by a matrix constructed from a structure tensor for matrix valued data. An important novelty is an intrinsically one-dimensional directional variant of the matrix-valued upwind schemes such as the Rouy-Tourin scheme. It enables our method to complete or enhance anisotropic structures effectively. A special advantage of our approach is that upwind schemes are utilised only in their basic one-dimensional version, hence avoiding grid effects and leading to an accurate algorithm. No higher dimensional variants of the schemes themselves are required. Experiments with synthetic and real-world data substantiate the gap-closing and line-completing properties of the proposed method.

B. Burgeth (✉) · L. Pizarro · M. Breuß · J. Weickert
Faculty of Mathematics and Computer Science, Saarland University, Saarbrücken, Germany
e-mail: burgeth@mia.uni-saarland.de

B. Burgeth
e-mail: burgeth@math.uni-sb.de

L. Pizarro
e-mail: pizarro@mia.uni-saarland.de

M. Breuß
e-mail: breuss@mia.uni-saarland.de

J. Weickert
e-mail: weickert@mia.uni-saarland.de

L. Pizarro
National Heart and Lung Institute, and Department of Computing, Imperial College London, South Kensington campus, London, UK
e-mail: l.pizarro@imperial.ac.uk

Keywords Mathematical morphology · PDEs · DT-MRI · Tensor field · Dilation · Erosion

1 Introduction

One of the primary tasks of mathematical morphology is the enhancement and extraction of shape information from image objects. This task is successfully tackled with a multitude of morphological operations based on the fundamental dilation and erosion processes. Dilation and erosion can be realised in a set-theoretic or ordering based framework, see e.g. (Matheron 1967, 1975; Serra 1967, 1982, 1988; Soille 2003), but it may also be implemented within the context of partial differential equations (PDE) (Alvarez et al. 1993; Arehart et al. 1993; Brockett and Maragos 1994; Sapiro et al. 1993; van den Boomgaard 1992) and their numerical solution schemes (see (Breuß and Weickert 2006) as well as the extensive list of literature cited there). The PDE-based approach is conceptually attractive since it allows for digital scalability and even adaptivity of the represented structuring element. This versatility was exploited, for example in Breuß et al. (2007) to create an adaptive, PDE-based dilation process for grey value images. In Burgeth et al. (2009b) the idea of morphological adaptivity has been transferred to the setting of matrix fields utilising the operator-algebraic framework proposed in Burgeth et al. (2007c). Matrix fields offer the opportunity of describing anisotropy in physical measurements and in image processing models, see Weickert and Hagen (2006), Laidlaw and Weickert (2009) for an overview. In diffusion tensor magnetic resonance imaging (DT-MRI), for example, information about the diffusive properties of water molecules is captured in symmetric positive definite matrices. The corresponding matrix field reflects the structure of the tissue under examination (Basser

et al. 1994). The goal of Burgeth et al. (2009b) was to enhance line-like and coherent structures in DT-MRI data. In this article we propose a concept for PDE-based adaptive morphology for matrix fields, involving directional derivatives in the formulation of the PDE-based dilation and erosion processes. In contrast to the approach in Burgeth et al. (2009b) and as a 3D-extension of the work in Pizarro et al. (2009) the numerical realisation employed in this article takes advantage of the accurate calculation of directional derivatives that relies on tri-linear interpolation.

We will start from a scalar adaptive formulation for d-dimensional data u in form of the dilation PDE

$$\partial_t u = \|M(u) \cdot \nabla u\| \tag{1}$$

with a data dependent, symmetric, positive semidefinite $d \times d$-matrix $M = M(u)$. Equation (1) describes a dilation with an ellipsoidal structuring element since an application of the mapping $(x, y, z)^\top \mapsto M \cdot (x, y, z)^\top$ transforms a sphere centered around the origin into an ellipsoid. When considering three-dimensional matrix-fields, for example, in DT-MRI data sets ($d = 3$) one has

$$M = \begin{pmatrix} a_{11} & a_{12} & a_{13} \\ a_{21} & a_{22} & a_{23} \\ a_{31} & a_{32} & a_{33} \end{pmatrix} = \begin{pmatrix} \|(a_{11}, a_{11}, a_{13})\| \nu^\top \\ \|(a_{21}, a_{21}, a_{23})\| \mu^\top \\ \|(a_{31}, a_{31}, a_{33})\| \eta^\top \end{pmatrix} \tag{2}$$

with unit vectors ν, μ, and η where, e.g.

$$\nu = \frac{1}{\|(a_{11}, a_{12}, a_{1,3})\|} \begin{pmatrix} a_{11} \\ a_{12} \\ a_{13} \end{pmatrix}. \tag{3}$$

This turns (1) into

$$\begin{aligned} \partial_t u = \Big(& (a_{11}\partial_x u + a_{12}\partial_y u + a_{13}\partial_z u)^2 \\ & + (a_{21}\partial_x u + a_{22}\partial_y u + a_{23}\partial_z u)^2 \\ & + (a_{31}\partial_x u + a_{32}\partial_y u + a_{33}\partial_z u)^2 \Big)^{\frac{1}{2}} \end{aligned} \tag{4}$$

$$\begin{aligned} = \Big(& \|(a_{11}, a_{12}, a_{13})\|^2 (\partial_\nu u)^2 \\ & + \|(a_{21}, a_{22}, a_{23})\|^2 (\partial_\mu u)^2 \\ & + \|(a_{31}, a_{32}, a_{33})\|^2 (\partial_\eta u)^2 \Big)^{\frac{1}{2}}. \end{aligned} \tag{5}$$

In Burgeth et al. (2009b) the partial derivatives $\partial_x u$, $\partial_y u$, and $\partial_z u$ in (4) were approximated with the standard Rouy-Tourin scheme (Rouy and Tourin 1992) in its two-dimensional version to obtain a directional derivative. However, in Pizarro et al. (2009) the directional derivatives necessary for the steering process were realised directly by means of (5) with better results than in Burgeth et al. (2009b). Hence it is decisive for our approach to implement the directional derivatives $\partial_\nu u$, $\partial_\mu u$, and $\partial_\eta u$ in (5) via a directional version of the Rouy-Tourin scheme as an upwind scheme suitable for the numerical solution of a transport equation (5). As it will be explained in Sect. 4 an important feature of the proposed approach is the fact that the upwind schemes are employed only in their simplest one-dimensional variant regardless of the dimensionality of the data set. No specially designed higher-dimensional versions or operator splitting methods have to be engaged.

This opens the path for using a high resolution method such as the flux-corrected-transport (FCT) scheme of Breuß and Weickert (2006) for which its 3D-version is not easily obtained in adaptive form in the setting of matrix fields. In total the novel features over Burgeth et al. (2009b) and Pizarro et al. (2009) are the realisation of higher morphological operators based on an adaptive directional version of the FCT scheme in three spatial dimensions.

The necessary directional information of the evolving u contained in the matrix $M(u)$ may be derived from the so-called structure tensor. The *structure tensor*, dating back to Förstner and Gülch (1987), Bigün et al. (1991), allows to extract directional information from an image. It is given by

$$S_\rho(u(x)) := G_\rho * \left(\nabla u(x) \cdot (\nabla u(x))^\top \right) \tag{6}$$

$$= \left(G_\rho * \left(\partial_{x_i} u(x) \cdot \partial_{x_j} u(x) \right) \right)_{i,j=1,\ldots,d}. \tag{7}$$

Here $G_\rho *$ indicates a convolution with a Gaussian of standard deviation ρ. For more details the reader is referred to Bigün (2006) and the literature cited therein. In Brox et al. (January 2006), Feddern et al. (2006) Di Zenzo's approach (Di Zenzo 1986) to construct a structure tensor for multichannel images has been extended to matrix fields yielding a *standard structure tensor*

$$J_\rho(U(x)) := \sum_{p,q=1}^{m} S_\rho(U_{p,q}(x)) \tag{8}$$

with $U = (U_{p,q})_{p,q=1,\ldots,m} \in \mathrm{Sym}_m(\mathbb{R})$, and $\mathrm{Sym}_m(\mathbb{R})$ denotes the set of symmetric $m \times m$-matrices with real entries. This tensor is a special case of the *full structure tensor concept* for matrix fields as proposed in Burgeth et al. (2009c). We will review this full structure concept in Sect. 2.

The article is structured as follows: In Sect. 2 we briefly give an account of basic notions of matrix analysis needed to establish a matrix-valued PDE for an adaptively steered morphological dilation process. We introduce the steering tensor that guides the dilation process adaptively in Sect. 3. It is explained how the numerical FCT scheme is turned into a directional variant that can be used on matrix fields in Sect. 4. Section 5 contains the definitions of the morphological operators we are going to extend in their directional versions to matrix fields. An evaluation of the performance of our approach to adaptive morphology for matrix fields is the subject of Sect. 6. The remarks in Sect. 7 conclude this article.

2 Matrix Analysis and an Extended Structure Tensor Concept

This section contains the key definitions for the formulation of matrix-valued PDEs. For a more detailed exposition the reader is referred to Burgeth et al. (2007c).

A matrix field is considered as a mapping $U : \Omega \subset \mathbb{R}^d \longrightarrow \mathrm{Sym}_m(\mathbb{R})$ from a d-dimensional image domain into the set of symmetric $m \times m$-matrices with real entries, $U(x) = (U_{p,q}(x))_{p,q=1,\ldots,m}$. The set of positive (semi-) definite matrices, denoted by $\mathrm{Sym}_m^{++}(\mathbb{R})$ (resp., $\mathrm{Sym}_m^{+}(\mathbb{R})$), consists of all symmetric matrices A with $\langle v, Av\rangle := v^\top Av > 0$ (resp., ≥ 0) for $v \in \mathbb{R}^m \setminus \{0\}$. This set is of special interest since DT-MRI produces data with this property. Note that at each point x the matrix $U(x)$ of a field of symmetric matrices can be diagonalised yielding $U(x) = V(x)^\top D(x)V(x)$, where $V(x)$ is a orthogonal matrix, while $D(x)$ is a diagonal matrix. In the sequel we will denote $m \times m$-diagonal matrices with entries $\lambda_1, \ldots, \lambda_m \in \mathbb{R}$ from left to right simply by $\mathrm{diag}(\lambda_1, \ldots, \lambda_m)$.

The extension of a function $h : \mathbb{R} \longrightarrow \mathbb{R}$ to $\mathrm{Sym}_m(\mathbb{R})$ is standard (Horn and Johnson 1990): With a slight abuse of notation we set $h(U) := V^\top \mathrm{diag}(h(\lambda_1), \ldots, h(\lambda_m))V \in \mathrm{Sym}_m^{+}(\mathbb{R})$, h denoting now a function acting on matrices as well. Observe that the systems of eigenvectors remains untouched. Specifying $h(s) = |s|, s \in \mathbb{R}$ as the absolut value function leads to the absolute value $|A| \in \mathrm{Sym}_m^{+}(\mathbb{R})$ of a matrix A. Similarly, multivariate functions $H : \mathbb{R}^m \longrightarrow \mathbb{R}^m$ can be extended in principle to symmetric matrices via $H(U) := V^\top \mathrm{diag}(H_1(\lambda_1 \ldots \lambda_m), \ldots, (H_m(\lambda_1 \ldots \lambda_m))V \in \mathrm{Sym}_m^{+}(\mathbb{R})$.

It is natural to define the partial derivative for matrix fields *componentwise*:

$$\overline{\partial}_\omega U = \left(\partial_\omega U_{p,q}\right)_{p,q=1,\ldots,m} \tag{9}$$

where $\omega \in \{t, x_1, \ldots, x_d\}$, that is, $\overline{\partial}_\omega$ stands for a spatial or temporal derivative. Viewing a matrix as a tensor (of second order), its gradient would be a third order tensor according to the rules of differential geometry. However, we adopt a more operator-algebraic point of view by defining the *generalised gradient* $\overline{\nabla}U(x)$ at a voxel $x = (x_1, \ldots, x_d)$ by

$$\overline{\nabla}U(x) := (\overline{\partial}_{x_1}U(x), \ldots, \overline{\partial}_{x_d}U(x))^\top \tag{10}$$

which is an element of $(\mathrm{Sym}_m(\mathbb{R}))^d$, in close analogy to the scalar setting where $\nabla u(x) \in \mathbb{R}^d$. For $W \in (\mathrm{Sym}_m(\mathbb{R}))^d$ we set $|W|_p := \sqrt[p]{|W_1|^p + \cdots + |W_d|^p}$ for $0 < p < +\infty$. It results in a positive semidefinite matrix from $\mathrm{Sym}_m^{+}(\mathbb{R})$, the direct counterpart of a nonnegative real number as the length of a vector in $\mathbb{R}^d$.

There will be the need for a symmetric multiplication of symmetric matrices. We opt for the so-called *Jordan product* $A \bullet B := \frac{1}{2}(AB + BA)$. It produces a symmetric matrix, it is commutative and distributive but not associative.

Furthermore, for later use in numerical schemes we have to clarify the notion of maximum and minimum of two symmetric matrices A, B. In direct analogy with relations known to be valid for real numbers one defines (Burgeth et al. 2007a):

$$\max(A, B) = \frac{1}{2}(A + B + |A - B|) \tag{11}$$

$$\min(A, B) = \frac{1}{2}(A + B - |A - B|) \tag{12}$$

where $|F|$ stands for the absolute value of the matrix F.

With this at our disposal we formulate the matrix-valued counterpart of (1) as

$$\overline{\partial}_t U = |\overline{M}(U) \bullet \overline{\nabla}U|_2 \tag{13}$$

with an initial matrix field $F(x) = U(x, 0)$. Here $\overline{M}(U)$ denotes a symmetric $md \times md$-block matrix with d^2 blocks of size $m \times m$ that is multiplied block-wise with $\overline{\nabla}U$ employing the Jordan product "$\bullet$". Note that $|\cdot|_2$ stands for the length of $\overline{M}(U) \bullet \overline{\nabla}U$ in the matrix valued sense. The construction of $\overline{M}(U)$ is detailed in Sect. 3 and relies on the full structure tensor.

The full structure tensor $\overline{S}_L$ for matrix fields as defined in Burgeth et al. (2009c) is used to extract directional information and it plays a vital role in the steering of evolution processes for matrix fields. It reads

$$\overline{S}_L(U) := G_\rho * \left(\overline{\nabla}U \cdot (\overline{\nabla}U)^\top\right) \tag{14}$$

$$= \left(G_\rho * \left(\overline{\partial}_{x_i}U \cdot \overline{\partial}_{x_j}U\right)\right)_{i,j=1,\ldots,d} \tag{15}$$

with $G_\rho *$ indicating a convolution with a Gaussian of standard deviation ρ.

$\overline{S}_L(U(x))$ is a symmetric $md \times md$-block matrix with d^2 blocks of size $m \times m$, $\overline{S}_L(U(x)) \in \mathrm{Sym}_d(\mathrm{Sym}_m(\mathbb{R})) = \mathrm{Sym}_{md}(\mathbb{R})$. Typically for the 3D medical DT-MRI data one has $d = 3$ and $m = 3$, yielding a 9×9-matrix $\overline{S}_L$. It can be diagonalised as $\overline{S}_L(U) = \sum_{k=1}^{md} \lambda_k w_k w_k^\top$ with real eigenvalues λ_k (w.l.o.g. arranged in decreasing order) and an orthonormal basis $\{w_k\}_{k=1,\ldots,md}$ of $\mathbb{R}^{md}$.

In order to extract useful d-dimensional directional information, $\overline{S}_L(U) \in \mathrm{Sym}_{md}(\mathbb{R})$ is reduced to a structure tensor $S(U) \in \mathrm{Sym}_d(\mathbb{R})$ in a generalised projection step (Burgeth et al. 2009c) using the block operator matrix $\mathrm{Tr}_A := \mathrm{diag}(\mathrm{tr}_A, \ldots, \mathrm{tr}_A)$ containing the trace operation. We set $\mathrm{Tr} := \mathrm{Tr}_{I_m}$ where I_m denotes the $m \times m$ unit matrix. This operator matrix acts on elements of the space $(\mathrm{Sym}_m(\mathbb{R}))^d$ as well as on block matrices via formal block-wise matrix multiplication,

$$\begin{pmatrix} \mathrm{tr}_A & \cdots & 0 \\ \vdots & \ddots & \vdots \\ 0 & \cdots & \mathrm{tr}_A \end{pmatrix} = \begin{pmatrix} M_{11} & \cdots & M_{1d} \\ \vdots & \ddots & \vdots \\ M_{d1} & \cdots & M_{dd} \end{pmatrix}$$

$$= \begin{pmatrix} \mathrm{tr}_A(M_{11}) & \cdots & \mathrm{tr}_A(M_{1d}) \\ \vdots & \ddots & \vdots \\ \mathrm{tr}_A(M_{d1}) & \cdots & \mathrm{tr}_A(M_{dd}) \end{pmatrix}, \tag{16}$$

provided that the square blocks M_{ij} have the same size as A. The projection that is conveyed by the reduction process condenses the directional information contained in $\overline{\mathcal{S}}_L(U)$, for a more detailed reasoning we must refer the reader to Burgeth et al. (2009c) for the sake of brevity. The reduction operation is accompanied by an extension operation: The I_m-extension is the mapping from $\mathrm{Sym}_d(\mathbb{R})$ to $\mathrm{Sym}_{md}(\mathbb{R})$ conveyed by the *Kronecker product* $\otimes$:

$$\begin{pmatrix} v_{11} & \cdots & v_{1d} \\ \vdots & \ddots & \vdots \\ v_{d1} & \cdot & v_{dd} \end{pmatrix} \longmapsto \begin{pmatrix} v_{11} & \cdots & v_{1d} \\ \vdots & \ddots & \vdots \\ v_{d1} & \cdots & v_{dd} \end{pmatrix} \otimes I_m \tag{17}$$

$$:= \begin{pmatrix} v_{11} I_m & \cdots & v_{1d} I_m \\ \vdots & \ddots & \vdots \\ v_{d1} I_m & \cdots & v_{dd} I_m \end{pmatrix}. \tag{18}$$

This resizing step renders a proper matrix-vector multiplication with the large generalised gradient $(\overline{\nabla} U(x))$ possible. By specifying the matrix A in (16) one may invoke a priori knowledge into the direction estimation (Burgeth et al. 2009c). The research on these structure-tensor concepts has been initiated by Weickert and Brox (2002), Brox et al. (January 2006). The approaches to matrix field regularisation suggested in Chefd'Hotel et al. (2002) are based on differential geometric considerations. Comprehensive survey articles on the analysis of matrix fields using various techniques can be found in Weickert and Hagen (2006).

3 Steering Matrix $\overline{M}(U)$ for Matrix Fields

With these notions we are in the position to propose the steering matrix $\overline{M}$ in the adaptive dilation process for matrix fields. We proceed in four steps:

1. The matrix field $\mathbb{R}^d \ni x \mapsto U(x)$ provides us with a module field of generalised gradients $\overline{\nabla} U(x)$ from which we construct the generalised structure tensor $\overline{\mathcal{S}}_L(U(x))$ possibly with a certain integration scale ρ. This step corresponds exactly to the scalar case.
2. We infer d-dimensional directional information by reducing $\overline{\mathcal{S}}_L(U(x))$ with tr_A with the help of the block operator matrix given in (16). This leads to a symmetric $d \times d$-matrix S, for example $S = J_\rho$ if $A = I_m$:

$$S(x) := \mathrm{Tr}_A\big(\overline{\mathcal{S}}_L(U(x))\big). \tag{19}$$

3. The symmetric $d \times d$-matrix S is spectrally decomposed, and the following mapping is applied:

$$H : \begin{cases} \mathbb{R}^d_+ \longrightarrow \mathbb{R}^d \\ (\lambda_1, \ldots, \lambda_d) \longmapsto \frac{1}{\sum_{i=1}^d \lambda_i}(c_1\lambda_1, \ldots, c_d\lambda_d) \end{cases} \tag{20}$$

where $c = (c_1, \ldots, c_d)$ is a vector with nonnegative entries. With the choice of the vector c we select the eigendirection in which the process is steered. For instance, specifying $c_1 = \cdots = c_{d-1} = k$ and $c_d = K \gg k$ one obtains an ellipsoid associated with the matrix M which is flipped if compared with S. Depending on the choice of K it can be more excentric than the one accompanying S. H applied to S yields the steering matrix M,

$$M := H(S). \tag{21}$$

4. Finally we enlarge the $d \times d$-matrix M to a $md \times md$-matrix $\overline{M}$ by the extension operation

$$\overline{M} = M \otimes I_m. \tag{22}$$

4 Directional Numerical Schemes in the Matrix-Valued Setting

For the numerical solution of nonlinear PDEs governing the dilation or erosion processes first-order finite difference methods such as the *Osher-Sethian scheme* (Osher and Fedkiw 2002; Osher and Sethian 1988; Sethian 1999) and the *Rouy-Tourin method* (Rouy and Tourin 1992; van den Boomgaard 1999) are popular choices. They are capable of correctly capturing propagating shocks, however, at the price of introducing some dissipation and blurring of edges. A remedy is provided by the flux-corrected transport (FCT) scheme introduced in Breuß and Weickert (2006) for scalar-valued morphology. By construction it utilises a first order-scheme as a primary step and then performs a careful correction of the introduced dissipation in a second step. In the subsequent two sections we sketch the *directional* versions of the Rouy-Tourin scheme and the FCT scheme with their extensions to the matrix-valued setting.

4.1 Directional form of the Rouy-Tourin Scheme

The first-order finite difference method of Rouy and Tourin (1992) may be used to solve the scalar PDE (5) in the *isotropic* case with $M = I_d$. Let us denote by $u^n_{i,j,k}$ the grey value of a scalar 3D image data set u at the pixel centered in $(ih_x, jh_y, kh_z) \in \mathbb{R}^3$ at the time-level $n\tau$ of the evolution. Furthermore, we employ standard forward, backward, and central difference operators, i.e.,

$$D^x_+ u^n_{i,j,k} := u^n_{i+1,j,k} - u^n_{i,j,k} \tag{23}$$

and

$$D_-^x u_{i,j,k}^n := u_{i,j,k}^n - u_{i-1,j,k}^n \tag{24}$$

and finally

$$D_c^x u_{i,j,k}^n := \left(u_{i+1,j,k}^n - u_{i-1,j,k}^n\right)/2 \tag{25}$$

here in x-, but analogously in y- and z-direction as well. The Rouy-Tourin method utilises an *upwind approximation* in the pixel (ih_x, jh_y, kh_z) of the partial derivative u_x (and analogously u_y, u_z):

$$u_x \approx \frac{1}{h_x}\max\left(\max\left(-D_-^x u_{i,j,k}^n, 0\right), \max\left(D_+^x u_{i,j,k}^n, 0\right)\right). \tag{26}$$

For a unit vector $\nu = (\nu_1, \nu_2, \nu_3)^\top$ the directional derivative $\partial_\nu u$ of u may be approximated by $\partial_\nu u = \langle \nu, \nabla u\rangle = \nu_1\partial_x u + \nu_2\partial_y u + \nu_3\partial_z u$. Hence it is close at hand to approximate numerically (4) directly. However, this favours mass transport along the directions of the x-, y-, and z-axis leading to a poor representation of the directional derivative. Instead we take advantage of (5) in this article and propose an alternative involving an interpolated function value $u_{i+\nu_1,j+\nu_2,k+\nu_3}$ defined by the subsequent well-known tri-linear[1] approximation (27) employing as weights the volumes of cuboids associated with the grid points (see also (Pizarro et al. 2009) in the bilinear case):

$$\begin{aligned}
&u_{i+\nu_1,j+\nu_2,k+\nu_3}\\
&\quad= u_{i,j,k}\cdot(1-h_x|\nu_1|)\cdot(1-h_y|\nu_2|)\cdot(1-h_z|\nu_3|)\\
&\qquad+ u_{i+\operatorname{sign}(\nu_1),j,k}\cdot h_x|\nu_1|\cdot(1-h_y|\nu_2|)\cdot(1-h_z|\nu_3|)\\
&\qquad+ u_{i,j+\operatorname{sign}(\nu_2),k}\cdot(1-h_x|\nu_1|)\cdot h_y|\nu_2|\cdot(1-h_z|\nu_3|)\\
&\qquad+ u_{i+\operatorname{sign}(\nu_1),j+\operatorname{sign}(\nu_2),k}\cdot h_x|\nu_1|\cdot h_y|\nu_2|\cdot(1-h_z|\nu_3|)\\
&\qquad+ u_{i,j,k+\operatorname{sign}(\nu_3)}\cdot(1-h_x|\nu_1|)\cdot(1-h_y|\nu_2|)\cdot h_z|\nu_3|\\
&\qquad+ u_{i+\operatorname{sign}(\nu_1),j,k+\operatorname{sign}(\nu_3)}\cdot h_x|\nu_1|\cdot(1-h_y|\nu_2|)\cdot h_z|\nu_3|\\
&\qquad+ u_{i,j+\operatorname{sign}(\nu_2),k+\operatorname{sign}(\nu_3)}\cdot(1-h_x|\nu_1|)\cdot h_y|\nu_2|\cdot h_z|\nu_3|\\
&\qquad+ u_{i+\operatorname{sign}(\nu_1),j+\operatorname{sign}(\nu_2),k+\operatorname{sign}(\nu_3)}\cdot h_x|\nu_1|\cdot h_y|\nu_2|\cdot h_z|\nu_3|.
\end{aligned} \tag{27}$$

This leads to forward and backward difference operators in the direction of ν with $\|\nu\| = \sqrt{\nu_1^2+\nu_2^2+\nu_3^2} = 1$:

$$D_+^\nu u_{i,j,k}^n := u_{i+\nu_1,j+\nu_2,k+\nu_3}^n - u_{i,j,k}^n \tag{28}$$

[1]For the sake of efficiency we use tri-linear interpolation, although higher order alternatives such as tri-cubic or spline interpolation can be employed as well.

$$D_-^\nu u_{i,j,k}^n := u_{i,j,k}^n - u_{i-\nu_1,j-\nu_2,k-\nu_3}^n \tag{29}$$

and to a direct approximation of the directional derivative

$$\begin{aligned}
\partial_\nu u &= u_\nu\\
&\approx \frac{1}{h}\max\left(\max\left(-D_-^\nu u_{i,j,k}^n, 0\right), \max\left(D_+^\nu u_{i,j,k}^n, 0\right)\right)
\end{aligned} \tag{30}$$

where $h := \min(h_x, h_y, h_z)$. Furthermore, the resulting approximation of the directional derivatives is also *c*onsistent: tri-linear approximation implies

$$\begin{aligned}
u_{i+\nu_1,j+\nu_2,k+\nu_3} &= u((i+\nu_1)h_x, (j+\nu_2)h_y, (k+\nu_3)h_z)\\
&\quad+ \mathcal{O}(\max(h_x, h_y, h_z)),
\end{aligned} \tag{31}$$

and hence we have

$$\begin{aligned}
&\frac{1}{h}D_+^\nu u_{i,j,k}\\
&= \frac{1}{h}\big(u((i+\nu_1)h_x, (j+\nu_2)h_y, (k+\nu_3)h_z)\\
&\quad- u(ih_x, jh_y, kh_z)\big) + \mathcal{O}(\max(h_x, h_y, h_z))
\end{aligned} \tag{32}$$

$$= u_\nu + \mathcal{O}(\max(h_x, h_y, h_z)). \tag{33}$$

Analogous reasoning applies to $D_-^\nu u_{i,j,k}$. With the calculus concept presented in Sect. 2 it is now straightforward to define one-sided directional differences in ν-direction for fields of $m \times m$-matrices:

$$\begin{aligned}
&D_+^\nu U^n(ih_x, jh_y, kh_z)\\
&\quad:= U^n((i+\nu_1)h_x, (j+\nu_2)h_y, (k+\nu_3)h_z)\\
&\qquad- U^n(ih_x, jh_y, kh_z)
\end{aligned} \tag{34}$$

$$\begin{aligned}
&D_-^\nu U^n(ih_x, jh_y, kh_z)\\
&\quad:= U^n(ih_x, jh_y, kh_z)\\
&\qquad- U^n((i-\nu_1)h_x, (j-\nu_2)h_y, (k-\nu_3)h_z)
\end{aligned} \tag{35}$$

where $D_+^\nu U^n$, $D_-^\nu U^n \in \mathrm{Sym}_m(\mathbb{R})$. In order to avoid confusion with the subscript notation for matrix components we wrote $U(ih_x, jh_y, kh_z)$ to indicate the (matrix-) value of the matrix field evaluated at the voxel centred at $(ih_x, jh_y, kh_z) \in \mathbb{R}^3$. The directions μ and η are treated accordingly. The notion of supremum and infimum of two matrices—as needed in a matrix variant of Rouy-Tourin—has been provided in Sect. 2 as well. Hence, having these generalisations at our disposal a directionally adaptive version of the Rouy-Tourin scheme is available now in the setting of matrix fields simply by replacing grey values $u_{i,j,k}^n$ by matrices $U^n(ih_x, jh_y, kh_z)$ and utilising the directional derivative approximations.

4.2 Directional FCT Scheme

The FCT scheme in its original version (Breuß and Weickert 2006) is by construction a new variant of a technique originally proposed by Boris and Book (1973, 1976, 1975) in the context of fluid flow simulation. As shown in Breuß and Weickert (2006), the FCT scheme results in accurate and (largely) rotationally invariant discrete representations of continuous-scale morphological dilation/erosion. For the sake of brevity we will not provide a derivation of the scalar FCT scheme since it can be found in detail in Breuß and Weickert (2006), see also Burgeth et al. (2009a) for its isotropic extension to matrix fields. We will also provide the directional modifications of the FCT method in the *two-dimensional* case only.

The basic idea of FCT is as follows. In a predictor step, the underlying PDE is solved by a simple and stable scheme usually afflicted with a fairly high diffusive numerical error. In a subsequent corrector step this error is negated by stabilised backward diffusion. The proposed FCT scheme relies on one-sided upwind differences as presented above. Using the Rouy-Tourin method as a *predictor*, denoting the result pointwise as $u_{i,j}^{n+1,\mathrm{pred}}$, the FCT method relies on a *corrector step*, which will finally read as

$$u_{i,j}^{n+1} = u_{i,j}^{n+1,\mathrm{pred}} + q_h^{n+1,\mathrm{pred}} - q_d^{n+1,\mathrm{pred}}. \tag{36}$$

One can identify the term $q_h^{n+1,\mathrm{pred}}$ in (36) as

$$q_h^{n+1,\mathrm{pred}} := \left(\left(\frac{\tau}{h_x} \left| D_c^x u_{i,j}^{n+1,\mathrm{pred}} \right| \right)^2 + \left(\frac{\tau}{h_y} \left| D_c^y u_{i,j}^{n+1,\mathrm{pred}} \right| \right)^2 \right)^{1/2}. \tag{37}$$

Here τ stands for the time step size of any explicit scheme usually employed to solve equations such as (1) numerically (see also Breuß and Weickert 2006; Burgeth et al. 2009a). For the term $q_d^{n+1,\mathrm{pred}}$ in (36) we make use of the quantities

$$g_{i+1/2,j} = \mathrm{mm}\left(D_-^x u_{i,j}^{n+1,\mathrm{pred}}, \frac{\tau}{2h_x} D_+^x u_{i,j}^{n+1,\mathrm{pred}}, D_+^x u_{i+1,j}^{n+1,\mathrm{pred}} \right) \tag{38}$$

$$g_{i,j+1/2} = \mathrm{mm}\left(D_-^y u_{i,j}^{n+1,\mathrm{pred}}, \frac{\tau}{2h_y} D_+^y u_{i,j}^{n+1,\mathrm{pred}}, D_+^y u_{i,j+1}^{n+1,\mathrm{pred}} \right) \tag{39}$$

where $\mathrm{mm}(\cdot,\cdot,\cdot)$ is the *scalar* minmod-function defined for three arguments as

$$\mathrm{mm}(a_1,a_2,a_3) := \begin{cases} \inf(a_1,a_2,a_3) & \text{for } a_1,a_2,a_3 > 0, \\ \sup(a_1,a_2,a_3) & \text{for } a_1,a_2,a_3 < 0, \\ 0 & \text{else.} \end{cases} \tag{40}$$

With these abbreviations we set

$$\delta^x u_{i,j}^{n+1,\mathrm{pred}} := \frac{\tau}{h_x} \left| D_c^x u_{i,j}^{n+1,\mathrm{pred}} \right| + g_{i+1/2,j} - g_{i-1/2,j} \tag{41}$$

$$\delta^y u_{i,j}^{n+1,\mathrm{pred}} := \frac{\tau}{h_y} \left| D_c^y u_{i,j}^{n+1,\mathrm{pred}} \right| + g_{i,j+1/2} - g_{i,j-1/2} \tag{42}$$

which finally yields the second new term in (36) as

$$q_d^{n+1,\mathrm{pred}} := \left(\left(\delta^x u_{i,j}^{n+1,\mathrm{pred}} \right)^2 + \left(\delta^y u_{i,j}^{n+1,\mathrm{pred}} \right)^2 \right)^{1/2}. \tag{43}$$

The directional version of the FCT-correction step (36) is now obtained by replacing the finite differences $D_{(\cdot)}^x$ in x-direction in (37) to (43) by the weighted finite differences $\|\hat{\nu}\| D_{(\cdot)}^{\nu}$ in ν-direction with $\hat{\nu} = (a_{11}, a_{12}, a_{13})$, see (2). We proceed in the same way with the other directions, substituting $D_{(\cdot)}^y$ by $\|\hat{\mu}\| D_{(\cdot)}^{\mu}$, and in the three-dimensional case, exchanging $D_{(\cdot)}^z$ by $\|\hat{\eta}\| D_{(\cdot)}^{\eta}$ with corresponding interpretations of $\hat{\mu}$ and $\hat{\eta}$. Together with the directional Rouy-Tourin scheme we obtain the directional version of the FCT method which is used in this article.

The non-directional FCT method has been successfully transfered to the setting of matrix fields in Burgeth et al. (2009a). So it is no surprise that the directional variant is readily extended to matrix fields. For details, especially concerning the matrix-valued counterpart of the minmod-function of three arguments by means of the Loewner ordering, the reader is referred to Burgeth et al. (2009a).

5 Morphological Operations

As indicated in the introduction the solution u of (1) mimics the dilation process with an adaptive ellipsoidal structuring element E which changes in time since it depends on u: $E = E_u$. Putting a minus sign on the right-hand-side of (1) gives the PDE-formulation of the corresponding adaptive erosion process. Using a common notation we express the dilation and the erosion of an original image f with such a structuring element E_u by

$$f \oplus E_u \quad \text{and} \quad f \ominus E_u. \tag{44}$$

The combinations of dilation and erosion lead to various morphological operators such as *opening* and *closing*,

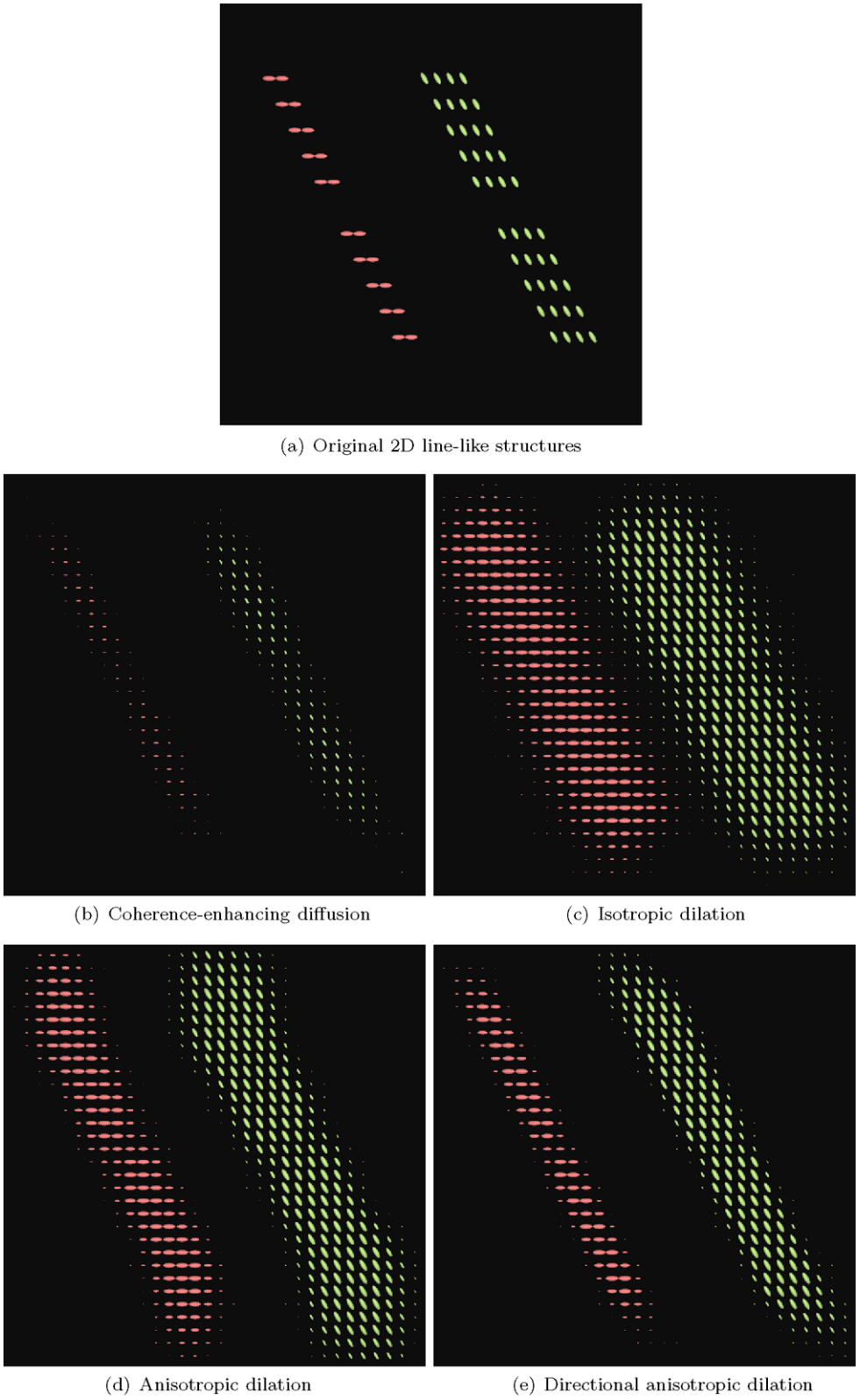

(a) Original 2D line-like structures

(b) Coherence-enhancing diffusion

(c) Isotropic dilation

(d) Anisotropic dilation

(e) Directional anisotropic dilation

Fig. 1 Comparison of different methods in 2D. (**a**) Original matrix field with ellipsoids in a line-like arrangement. (**b**) Coherence-enhancing diffusion (CED) with $\rho = 4$, $t = 3$. (**c**) Isotropic (classical) dilation at $t = 3$ using the Rouy-Tourin scheme. (**d**) and (**e**) show the proposed adaptive, anisotropic dilation using the classical Rouy-Tourin scheme as in Burgeth et al. (2009b) and the *directional* Rouy-Tourin scheme, respectively, with $\rho = 4$, $c = (0.2, 20)$, $t = 1$

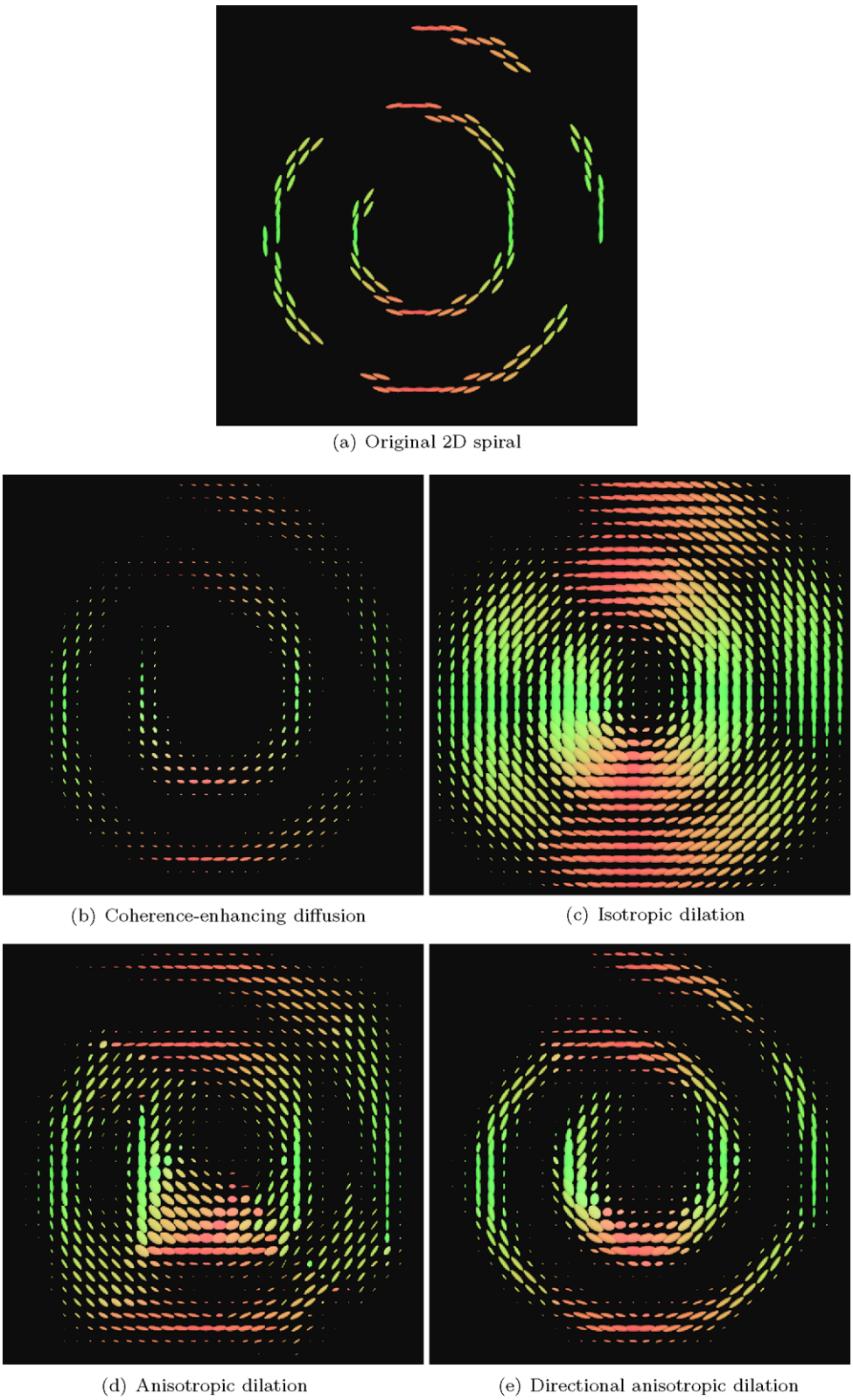

(a) Original 2D spiral

(b) Coherence-enhancing diffusion

(c) Isotropic dilation

(d) Anisotropic dilation

(e) Directional anisotropic dilation

Fig. 2 Comparison of different methods in 2D. (**a**) Original spiral with missing tensors. (**b**) Coherence-enhancing diffusion (CED) with $\rho = 3$, $t = 6$. (**c**) Isotropic dilation at $t = 3$ using the Rouy-Tourin scheme. (**d**) and (**e**) show the proposed adaptive, anisotropic dilation using the classical Rouy-Tourin scheme as in Burgeth et al. (2009b) and the *directional* Rouy-Tourin scheme, respectively, with $\rho = 3$, $c = (0.2, 20)$, $t = 1$

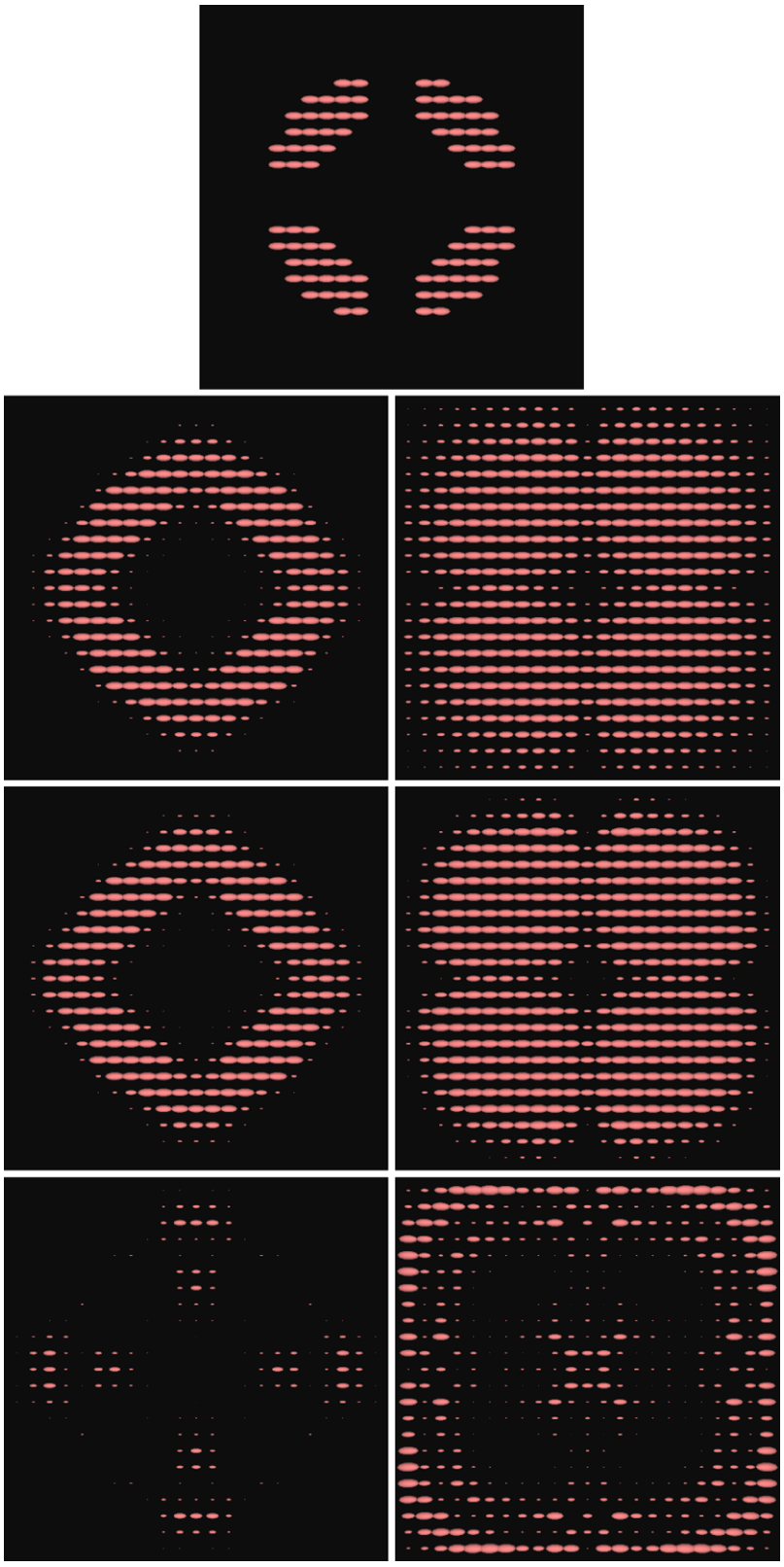

Fig. 3 *Top row:* Synthetic 2D circle with missing information. *Second row:* From left to right: Dilation with *directional* Rouy-Tourin scheme in the tangential direction and in the radial direction. *Third row:* The same using the *directional* FCT scheme. *Bottom row:* Scaled absolute differences between both schemes

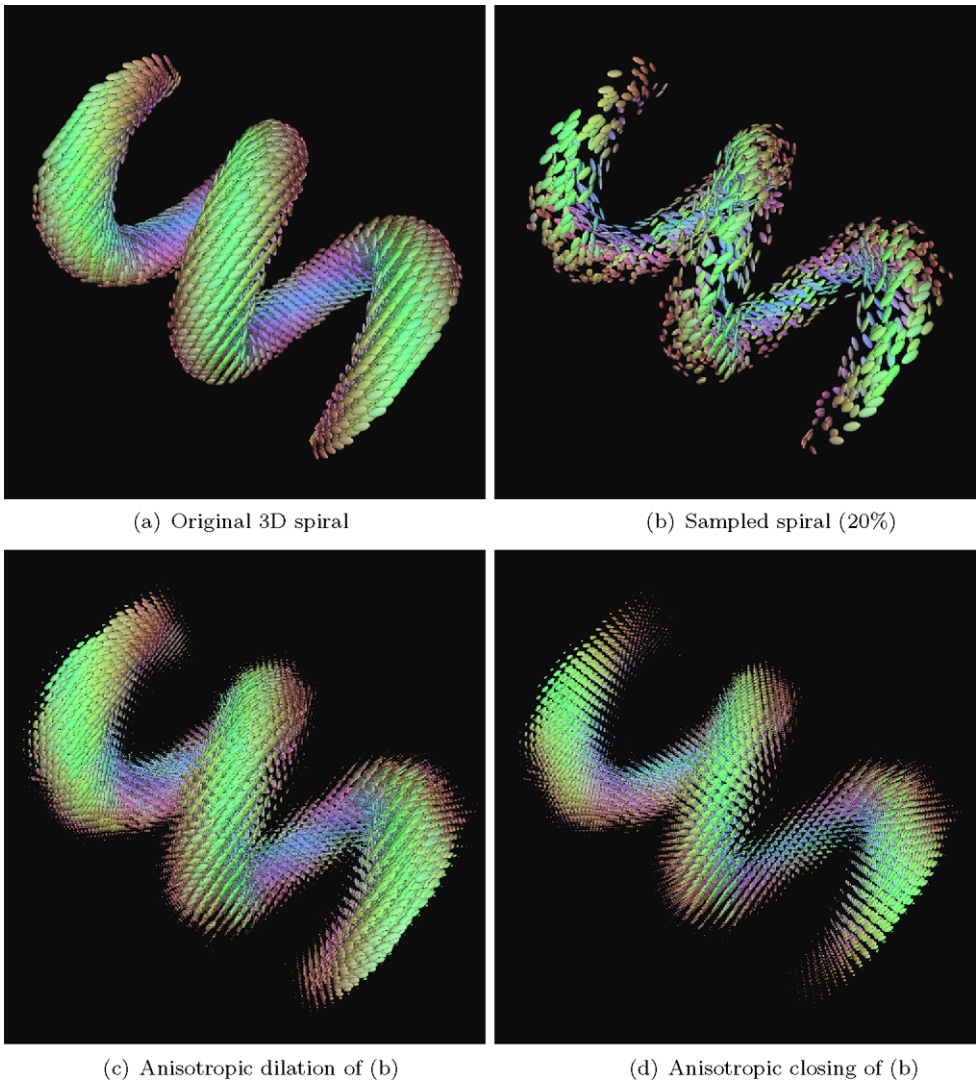

(a) Original 3D spiral (b) Sampled spiral (20%)

(c) Anisotropic dilation of (b) (d) Anisotropic closing of (b)

Fig. 4 Adaptive, anisotropic dilation and closing in 3D using the *directional* FCT scheme with parameters $\rho = 2$, $c = (0.2, 0.2, 20)$, $t = 5$

$$f \circ E_u := (f \ominus E_u) \oplus E_u, \tag{45}$$

$$f \bullet E_u := (f \oplus E_u) \ominus E_u. \tag{46}$$

In an image, boundaries of objects are loci of high grey value variations, and as such they can be detected by derivative operators. The so-called *Beucher gradient*

$$\varrho_{E_u}(f) := (f \oplus E_u) - (f \ominus E_u), \tag{47}$$

as well as the *internal* and *external gradient*,

$$\begin{aligned} \varrho^-_{E_u}(f) &:= f - (f \ominus E_u), \\ \varrho^+_{E_u}(f) &:= (f \oplus E_u) - f, \end{aligned} \tag{48}$$

are morphological counterparts of the norm of the gradient f, $\|\nabla f\|$, if f is considered as a differentiable image.

In van Vliet et al. (1989) a *morphological Laplacian* has been introduced. We define a variant by

$$\Delta_{E_u} f := \varrho^+_{E_u}(f) - \varrho^-_{E_u}(f) \tag{49}$$

$$= (f \oplus E_u) - 2 \cdot f + (f \ominus E_u). \tag{50}$$

This Laplacian is a morphological equivalent of the second derivative $\partial_{\eta\eta} f$ where η stands for the unit vector in the direction of the steepest slope. It allows us to distinguish between influence zones of minima and maxima of the image f. This is a vital property for the construction of so-called *s*hock filters (Guichard and Morel 2003; Kramer and Bruckner 1975; Osher and Rudin 1990). Shock filtering amounts to applying either a dilation or an erosion to an image, depending on whether the pixel is located within the influence zone of a minimum or a maximum:

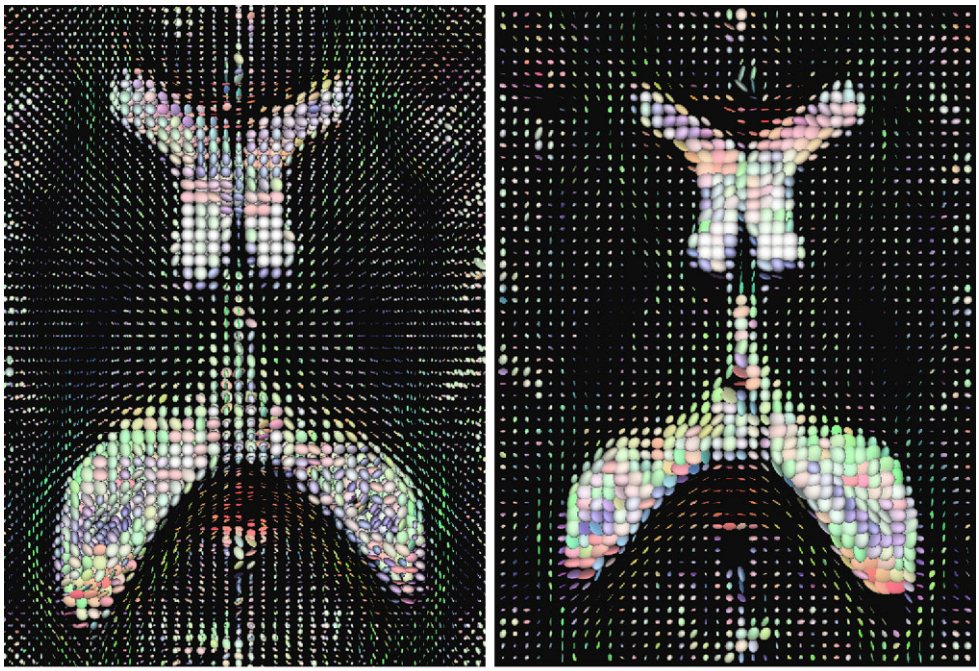

(a) Original 3D section of DT-MRI data (b) 2D slice with 40×55 matrices

Fig. 5 Real world data used in our experiments

$$S_{E_u} f := \begin{cases} f \oplus E_u, & \Delta_{E_u} f < 0, \\ f, & \Delta_{E_u} f = 0, \\ f \ominus E_u, & \Delta_{E_u} f > 0. \end{cases} \tag{51}$$

A considerable number of variants of shock filters have been considered in the literature (Alvarez and Mazorra 1994; Gilboa et al. 2002; Osher and Rudin 1991; Remaki and Cheriet 2003; Schavemaker et al. 1997; Weickert 2003). When they are applied iteratively, experiments show that their steady state is given by a piecewise constant image with discontinuities ("shocks") between adjacent segments of constant grey value. For more details about the morphological shock filter as introduced above, see Burgeth et al. (2007b).

In the experimental Sect. 6 we will see the results obtained by the various adaptive, PDE-driven morphological operators when applied to 2D and 3D matrix fields.

6 Experiments

The matrix data are visualised as an ellipsoid in each voxel via the level sets of quadratic form $\{v \in \mathbb{R}^3 : v^\top U^{-2}(i, j, k)v = const.\}$. It is associated with the matrix $U(i, j, k) \in \mathrm{Sym}_3^+(\mathbb{R})$ representing the matrix field at voxel (ih_x, jh_y, kh_z). By using U^{-2} the length of the semi-axes of the ellipsoid correspond directly with the three eigenvalues of the matrix. Changing the constant *const.* amounts to a mere scaling of the ellipsoids. Note that only positive definite matrices produce ellipsoids as level sets of its quadratic form.

In the following we employ the Rouy-Tourin scheme, the FCT scheme, and their corresponding directional versions. In all schemes we use a grid size $h_x = h_y = h_z = 1$.

6.1 Synthetic Data in 2D and 3D

Figure 1(a) exhibits a 32×32 matrix field composed of two interrupted diagonal stripes with different thickness, both built with cigar-shaped ellipsoids of equal size but different orientation. The line-like structures are tilted with respect to the x-axis by an angle of about 117 degrees. Figure 1(b) shows the result of applying coherence-enhancing diffusion (CED) (Burgeth et al. 2009c). Figure 1(c) contains the result of isotropic (classical) dilation (Burgeth et al. 2007a) using the standard (non-directional) Rouy-Tourin scheme. Figure 1(d) and Fig. 1(e) show the result of the proposed adaptive anisotropic dilation using the Rouy-Tourin scheme in its standard and directional versions, respectively. The parameters used were chosen in a way that every method fills in the missing tensors of both stripes. Our approach is able to complete the line-like structures much faster and more accurate than the other methods. A noticeable improvement is introduced by the directional numerical scheme, which overcomes the numerical bias towards the coordinate axes of classical upwind schemes (e.g. Rouy-Tourin). Moreover, note that the direction and amount of adaptive anisotropic dilation does not depend on the orientation of the ellipsoids, but on the orientation and width of the structures. It is worth mentioning that the CED approach decreases the overall size of matrices since the total mass, that is, the volume of the ellipsoids is only redistributed due to the property of mass

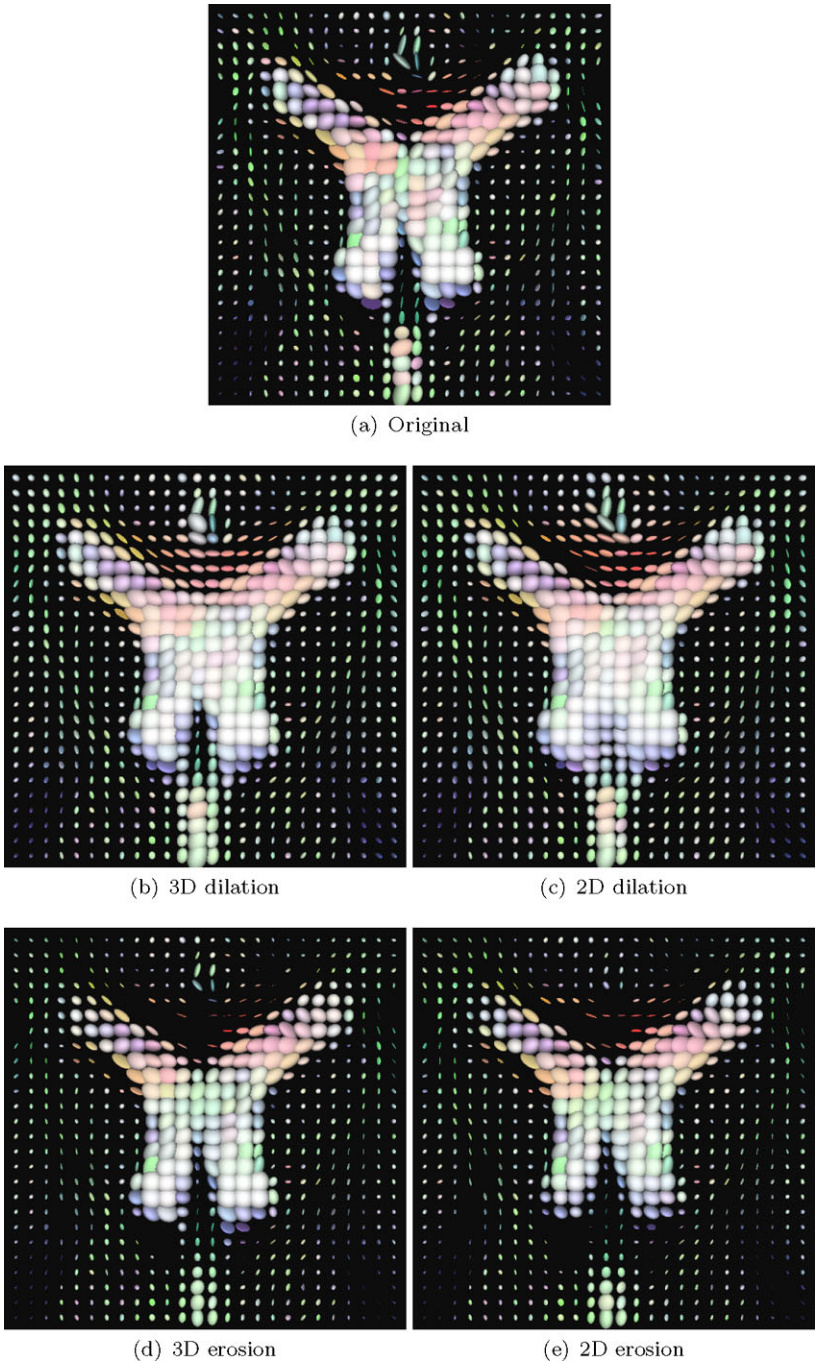

Fig. 6 Adaptive, anisotropic dilation and erosion in 3D and 2D using the *directional* FCT scheme with parameters $\rho = 1$, $c = (0.05, 0.05, 5)$, $t = 3$ in the 3D case, and $\rho = 1$, $c = (0.05, 5)$, $t = 1$ in the 2D case

conservation. The same experiment is performed on a 2D spiral data set with missing information, whose outcome is depicted in Fig. 2. Again, only the anisotropic dilation succeeds to close the gaps satisfactorily preserving the spiral structure of the object. As expected, the adaptive dilation process is faster than the diffusion based method and the classical isotropic dilation. Furthermore, the effect of employing a directional numerical scheme becomes more evident when the anisotropic dilation is steered along circular structures.

We now use both the *directional* Rouy-Tourin scheme and the *directional* FCT scheme for dilating the test image with an interrupted circular structure shown at the top of Fig. 3. In the first test the dilation process is steered in tangential direction while in a second test the radial direction is selected via the choice of the parameter $c = (c_1, c_2)$, namely $c = (0.1, 10)$ in the first case and $c = (10, 0.1)$ in the second one. Both directional schemes were applied, the results together with a scaled ($\times 5$) absolute difference image are depicted in Fig. 3. As expected the directional FCT

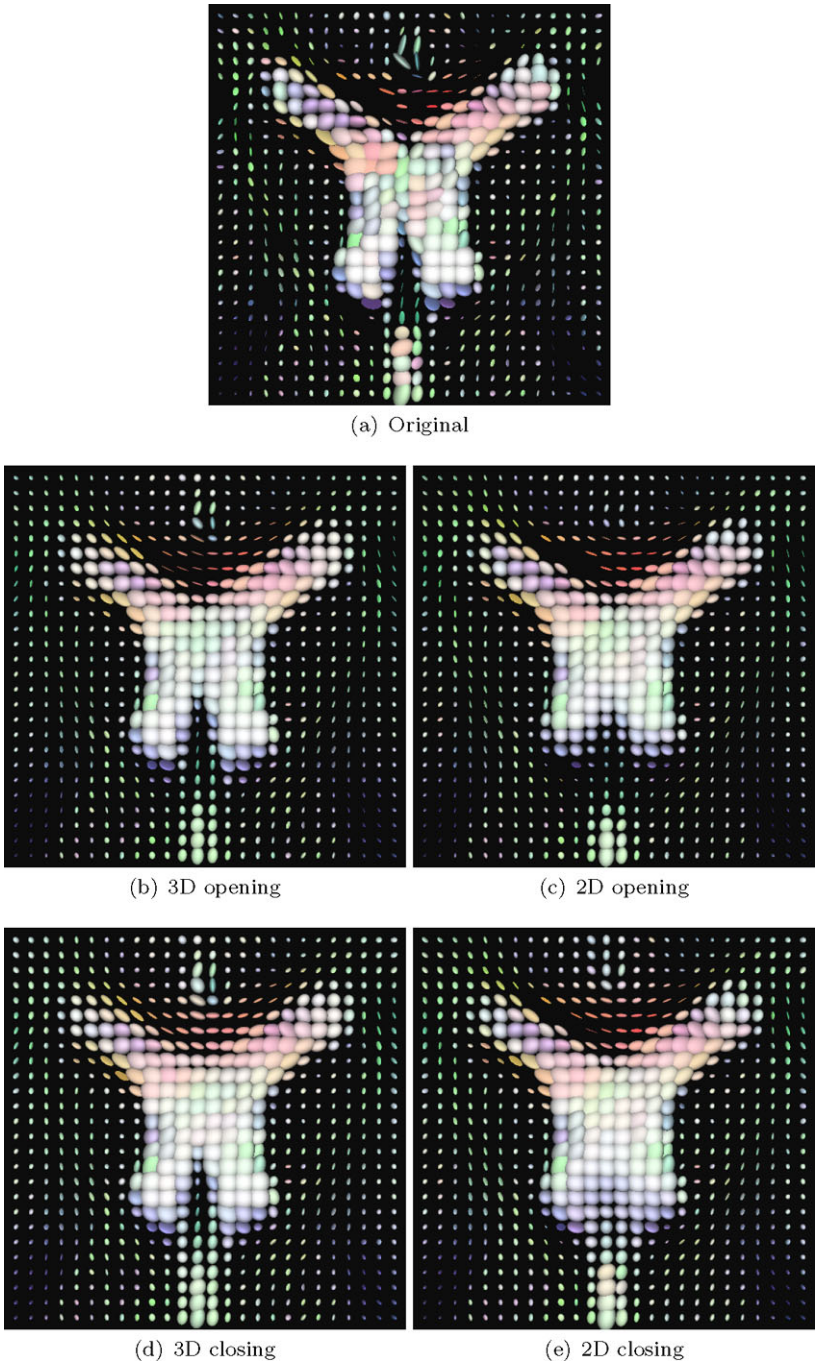

(a) Original

(b) 3D opening (c) 2D opening

(d) 3D closing (e) 2D closing

Fig. 7 Adaptive, anisotropic opening and closing in 3D and 2D using the *directional* FCT scheme with parameters $\rho = 1$, $c = (0.05, 0.05, 5)$, $t = 3$ in the 3D case, and $\rho = 1$, $c = (0.05, 5)$, $t = 1$ in the 2D case

method performs favourable in terms of edge preservation over the directional Rouy-Tourin scheme. This can be seen in the difference images at the bottom of Fig. 3, which display the (scaled) dissipation introduced by the Rouy-Tourin scheme that has been corrected by the FCT scheme.

A much more elaborate matrix field can be seen in Fig. 4(a). This 3D data set[2] is sparsified by removing 80% of the matrices (Fig. 4(b)). Both adaptive anisotropic dilation (Fig. 4(c)) and closing (Fig. 4(d)) performed with the superior *directional* FCT scheme, provide a reasonable reconstruction of the original data.

6.2 Real World Data: 3D DT-MRI

We also tested the proposed method on a real DT-MRI data set of a human head consisting of a $128 \times 128 \times 38$-field of positive definite matrices. Figure 5(a) displays part of the

[2]The 3D spiral data set is freely available as part of the Teem toolkit at http://teem.sourceforge.net.

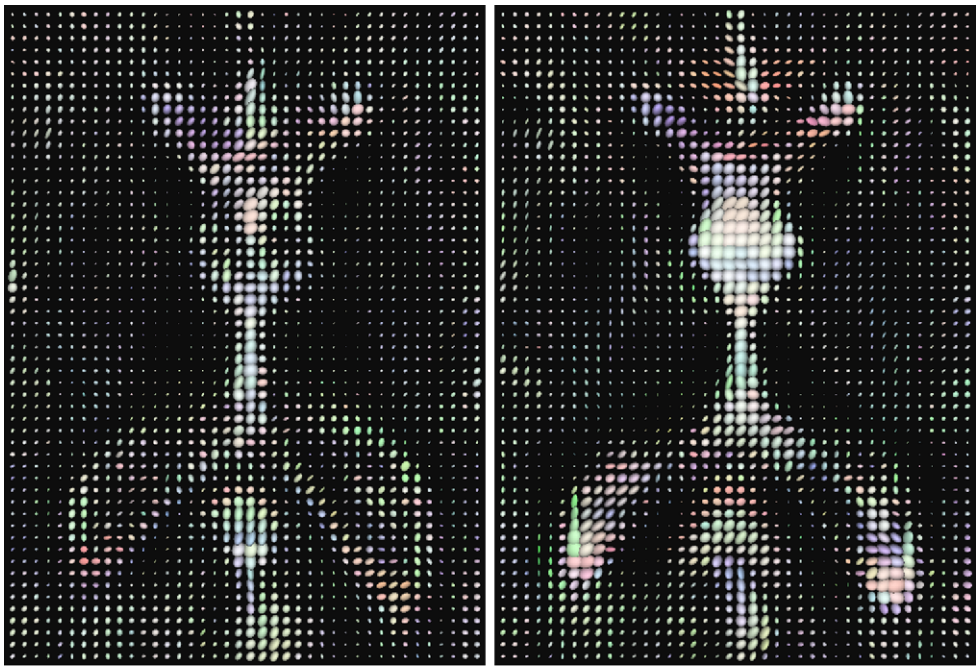

(a) 3D Beucher gradient (b) 2D Beucher gradient

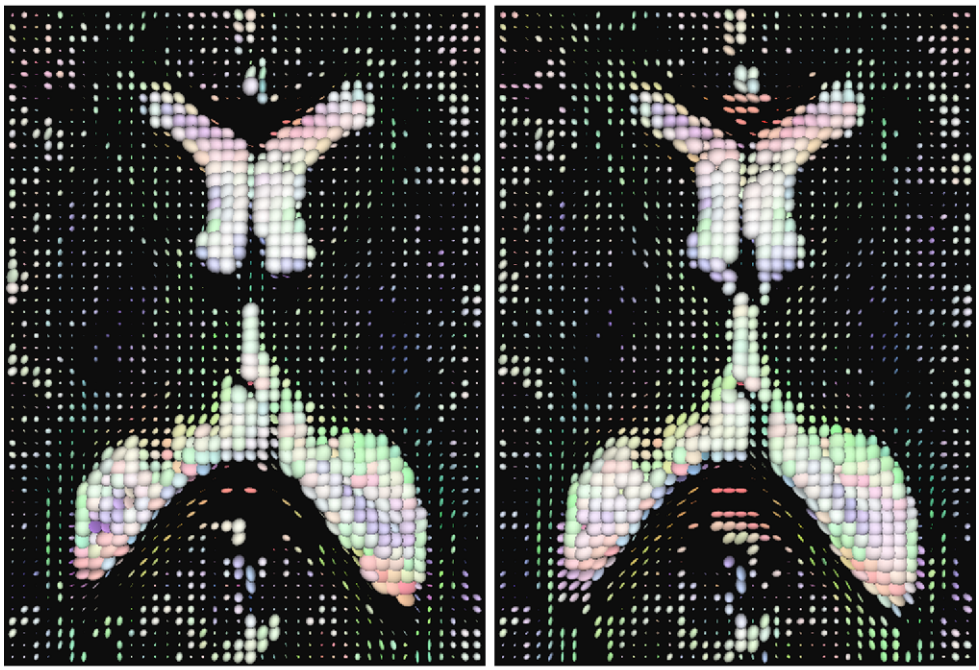

(c) 3D shock filtering (d) 2D shock filtering

Fig. 8 Adaptive, anisotropic Beucher gradient and shock filtering in 3D and 2D using the *directional* FCT scheme with parameters $\rho = 1$, $c = (0.1, 0.1, 10)$, $t = 5$ in the 3D case, and $\rho = 1$, $c = (0.1, 10)$, $t = 2$ in the 2D case

lateral ventricles as an actual three-dimensional $40 \times 55 \times 3$-data set while Fig. 5(b) shows only a 2D-slice. In the experiments on real-world data we will always juxtapose the results of various adaptive morphological operations when applied to 2D-slices and truly 3D data. However, in order to avoid visual cluttering, we will in general extract and depict from the processed 3D data an appropriate 2D-slice only. Note that we use for the adaptive morphological operations from now on only the directional FCT scheme in its 3D and 2D realisations.

In Fig. 6 we zoom into the lateral ventricles to show the effect of applying adaptive dilation and erosion in both the 3D and 2D setting. We see that the adaptive dilation and erosion processes on matrix fields respect the underlying shape of the ventricles if compared to the isotropic case (Burgeth et al. 2009a). We notice that the results are quite similar in

the 3D and in the 2D setting. However, the 3D process seems to be more accurate at the price of a longer evolution time ($t = 3$), than in the 2D case ($t = 1$).

The lateral ventricles serve also as a test case for the reconstructing operations of adaptive opening and closing, Fig. 7. In 3D the lateral ventricles are nicely recovered in a slightly simplified form, as expected, since the processes incorporate also information from neighbouring slices.

The difference in processing of 2D and 3D data sets becomes prominent in the case of the morphological derivatives, e.g. the Beucher gradient. The gradient operations detect the boundary of the ventricles, which are three-dimensional anatomical structures. This boundary in a cross-section can be seen clearly in Fig. 8(a). In contrast to this, the boundaries are less localised in the 2D case, Fig. 8(b).

For the adaptive version of the morphological shock filter we obtain the matrix valued equivalent of a piece-wise constant image both in the 3D and the 2D case. In the three-dimensional setting, Fig. 8(c), we observe a slightly better localisation of the shock segments than in 2D, Fig. 8(d).

7 Conclusion

We have presented a method for an adaptive, PDE-based dilation and erosion processes in the setting of matrix fields. The evolution governed by matrix-valued PDEs is guided by a steering tensor whose construction relies on the full structure tensor for matrix data.

In order to enable proper directional steering we extended the schemes of Rouy-Tourin and the FCT method in two ways: First, turning them into directional schemes based on directional finite differences via interpolation. Second, by means of advanced matrix calculus, extending these directional variants to matrix fields solving the matrix-valued adaptive PDEs of dilation and erosion. Having these two key operations at our disposal we were able to propose higher order morphological operators such as morphological derivatives that are adaptive and act on matrix fields.

As a proof-of-concept we applied these adaptive morphological operations to synthetic and real DT-MRI data. The tests reveal that the various adaptive morphological operators behave as one might expected from their scalar counterparts. For instance, the adaptive dilation and closing are indeed capable of filling in missing data and to complete directional structures. We also confirmed that the FCT performs preferable over the scheme of Rouy and Tourin.

The direct application of an elementary morphological operation is usually not suitable for improving an image or extracting useful information from it. Morphology (adaptive or not) gains its power from the capability of concatenating and combining elementary operations according to the task at hand. We hope to have just opened the adaptive morphological toolbox for matrix fields. In this respect the proposed approach to adaptive morphology for matrix fields may have its merits, for example, in the segmentation of directional structures or as a preprocessing step for fiber tracking algorithms in medical imaging.

Acknowledgements L.P. gratefully acknowledges partial funding by the German Academic Exchange Service (DAAD), grant no. A/05/21715.

The DT-MRI data set has been provided by Anna Vilanova i Bartoli, Eindhoven University of Technology.

We thank Thomas Schultz (Max-Planck Institute for Computer Science) for his help in formatting the 3D spiral data set.

We thank the anonymous reviewers for their valuable comments that helped to improve this paper.

References

Alvarez, L., & Mazorra, L. (1994). Signal and image restoration using shock filters and anisotropic diffusion. *SIAM Journal on Numerical Analysis*, *31*, 590–605.

Alvarez, L., Guichard, F., Lions, P.-L., & Morel, J.-M. (1993). Axioms and fundamental equations in image processing. *Archive for Rational Mechanics and Analysis*, *123*, 199–257.

Arehart, A. B., Vincent, L., & Kimia, B. B. (1993). Mathematical morphology: The Hamilton–Jacobi connection. In *Proc. fourth international conference on computer vision* (pp. 215–219). Berlin, May 1993. New York: IEEE Computer Society Press.

Basser, P. J., Mattiello, J., & LeBihan, D. (1994). MR diffusion tensor spectroscopy and imaging. *Biophysical Journal*, *66*, 259–267.

Bigün, J. (2006). *Vision with direction*. Berlin: Springer.

Bigün, J., Granlund, G. H., & Wiklund, J. (1991). Multidimensional orientation estimation with applications to texture analysis and optical flow. *IEEE Transactions on Pattern Analysis and Machine Intelligence*, *13*(8), 775–790.

Boris, J. P., & Book, D. L. (1973). Flux corrected transport. I. SHASTA, a fluid transport algorithm that works. *Journal of Computational Physics*, *11*(1), 38–69.

Boris, J. P., & Book, D. L. (1976). Flux corrected transport. III. Minimal error FCT algorithms. *Journal of Computational Physics*, *20*, 397–431.

Boris, J. P., Book, D. L., & Hain, K. (1975). Flux corrected transport. II. Generalizations of the method. *Journal of Computational Physics*, *18*, 248–283.

Breuß, M., & Weickert, J. (2006). A shock-capturing algorithm for the differential equations of dilation and erosion. *Journal of Mathematical Imaging and Vision*, *25*(2), 187–201.

Breuß, M., Burgeth, B., & Weickert, J. (2007). Anisotropic continuous-scale morphology. In J. Martí, J. M. Benedí, A. M. Mendonça, & J. Serrat (Eds.), *Lecture notes in computer science: Vol. 4478. Pattern recognition and image analysis* (pp. 515–522). Berlin: Springer.

Brockett, R. W., & Maragos, P. (1994). Evolution equations for continuous-scale morphological filtering. *IEEE Transactions on Signal Processing*, *42*, 3377–3386.

Brox, T., Weickert, J., Burgeth, B., & Mrázek, P. (2006). Nonlinear structure tensors. *Image and Vision Computing*, *24*(1), 41–55.

Burgeth, B., Bruhn, A., Didas, S., Weickert, J., & Welk, M. (2007a). Morphology for matrix-data: Ordering versus PDE-based approach. *Image and Vision Computing*, *25*(4), 496–511.

Burgeth, B., Bruhn, A., Papenberg, N., Welk, M., & Weickert, J. (2007b). Mathematical morphology for tensor data induced by the Loewner ordering in higher dimensions. *Signal Processing*, *87*(2), 277–290.

Burgeth, B., Didas, S., Florack, L., & Weickert, J. (2007c). A generic approach to diffusion filtering of matrix-fields. *Computing*, *81*, 179–197.

Burgeth, B., Breuß, M., Didas, S., & Weickert, J. (2009a). PDE-based morphology for matrix fields: Numerical solution schemes. In S. Aja-Fernández, R. de Luis García, D. Tao, & X. Li (Eds.), *Advances in pattern recognition. Tensors in image processing and computer vision* (pp. 125–150). London: Springer.

Burgeth, B., Breuß, M., Pizarro, L., & Weickert, J. (2009b). PDE-driven adaptive morphology for matrix fields. In X.-C. Tai et al. (Eds.), *Lecture notes in computer science: Vol. 5567. Proc. of the second international conference on scale space and variational methods in computer vision* (pp. 247–258). Berlin: Springer.

Burgeth, B., Didas, S., & Weickert, J. (2009c). A general structure tensor concept and coherence-enhancing diffusion filtering for matrix fields. In D. Laidlaw & J. Weickert (Eds.), *Mathematics and visualization. Visualization and processing of tensor fields* (pp. 305–323). Berlin: Springer.

Chefd'Hotel, C., Tschumperlé, D., Deriche, R., & Faugeras, O. (2002). Constrained flows of matrix-valued functions: Application to diffusion tensor regularization. In A. Heyden, G. Sparr, M. Nielsen, & P. Johansen (Eds.), *Lecture notes in computer science: Vol. 2350. Computer vision—ECCV 2002* (pp. 251–265). Berlin: Springer.

Di Zenzo, S. (1986). A note on the gradient of a multi-image. *Computer Vision, Graphics and Image Processing*, *33*, 116–125.

Feddern, C., Weickert, J., Burgeth, B., & Welk, M. (2006). Curvature-driven PDE methods for matrix-valued images. *International Journal of Computer Vision*, *69*(1), 91–103.

Förstner, W., & Gülch, E. (1987). A fast operator for detection and precise location of distinct points, corners and centres of circular features. In *Proc. ISPRS intercommission conference on fast processing of photogrammetric data* (pp. 281–305). Interlaken, Switzerland, June 1987.

Gilboa, G., Sochen, N. A., & Zeevi, Y. Y. (2002). Regularized shock filters and complex diffusion. In A. Heyden, G. Sparr, M. Nielsen, & P. Johansen (Eds.), *Lecture notes in computer science: Vol. 2350. Computer vision—ECCV 2002* (pp. 399–413). Berlin: Springer.

Guichard, F., & Morel, J.-M. (2003). A note on two classical enhancement filters and their associated PDE's. *International Journal of Computer Vision*, *52*(2/3), 153–160.

Horn, R. A., & Johnson, C. R. (1990). *Matrix analysis*. Cambridge: Cambridge University Press.

Kramer, H. P., & Bruckner, J. B. (1975). Iterations of a non-linear transformation for enhancement of digital images. *Pattern Recognition*, *7*, 53–58.

Laidlaw, D., & Weickert, J. (Eds.) (2009). *Visualization and processing of tensor fields*. Berlin: Springer.

Matheron, G. (1967). *Eléments pour une théorie des milieux poreux*. Paris: Masson.

Matheron, G. (1975). *Random sets and integral geometry*. New York: Wiley.

Osher, S., & Fedkiw, R. P. (2002). *Applied mathematical sciences: Vol. 153. Level set methods and dynamic implicit surfaces*. New York: Springer.

Osher, S., & Rudin, L. I. (1990). Feature-oriented image enhancement using shock filters. *SIAM Journal on Numerical Analysis*, *27*, 919–940.

Osher, S., & Rudin, L. (1991). Shocks and other nonlinear filtering applied to image processing. In A. G. Tescher (Ed.), *Proceedings of SPIE: Vol. 1567. Applications of digital image processing XIV* (pp. 414–431). Bellingham: SPIE Press.

Osher, S., & Sethian, J. A. (1988). Fronts propagating with curvature-dependent speed: Algorithms based on Hamilton–Jacobi formulations. *Journal of Computational Physics*, *79*, 12–49.

Pizarro, L., Burgeth, B., Breuß, M., & Weickert, J. (2009). A directional Rouy-Tourin scheme for adaptive matrix-valued morphology. In M. H. F. Wilkinson & J. B. T. M. Roerdink (Eds.), *Lecture notes in computer science: Vol. 5720. Proc. of the ninth international symposium on mathematical morphology, ISMM* (pp. 250–260). Berlin: Springer.

Remaki, L., & Cheriet, M. (2003). Numerical schemes of shock filter models for image enhancement and restoration. *Journal of Mathematical Imaging and Vision*, *18*(2), 153–160.

Rouy, E., & Tourin, A. (1992). A viscosity solutions approach to shape-from-shading. *SIAM Journal on Numerical Analysis*, *29*, 867–884.

Sapiro, G., Kimmel, R., Shaked, D., Kimia, B. B., & Bruckstein, A. M. (1993). Implementing continuous-scale morphology via curve evolution. *Pattern Recognition*, *26*, 1363–1372.

Schavemaker, J. G. M., Reinders, M. J. T., & van den Boomgaard, R. (1997). Image sharpening by morphological filtering. In *Proc. 1997 IEEE workshop on nonlinear signal and image processing*, Mackinac Island, MI, September 1997. www.ecn.purdue.edu/NSIP/.

Serra, J. (1967). *Echantillonnage et estimation des phénomènes de transition minier*. PhD thesis, University of Nancy, France.

Serra, J. (1982). *Image analysis and mathematical morphology* (Vol. 1). London: Academic Press.

Serra, J. (1988). *Image analysis and mathematical morphology* (Vol. 2). London: Academic Press.

Sethian, J. A. (1999). *Level set methods and fast marching methods* (2nd ed.). Cambridge: Cambridge University Press. Paperback edition.

Soille, P. (2003). *Morphological image analysis* (2nd ed.). Berlin: Springer.

van den Boomgaard, R. (1992). *Mathematical morphology: Extensions towards computer vision*. PhD thesis, University of Amsterdam, The Netherlands.

van den Boomgaard, R. (1999). Numerical solution schemes for continuous-scale morphology. In M. Nielsen, P. Johansen, O. F. Olsen, & J. Weickert (Eds.), *Lecture notes in computer science: Vol. 1682. Scale-space theories in computer vision* (pp. 199–210). Berlin: Springer.

van Vliet, L. J., Young, I. T., & Beckers, A. L. D. (1989). A nonlinear Laplace operator as edge detector in noisy images. *Computer Vision, Graphics and Image Processing*, *45*(2), 167–195.

Weickert, J. (2003). Coherence-enhancing shock filters. In B. Michaelis & G. Krell (Eds.), *Lecture notes in computer science: Vol. 2781. Pattern recognition* (pp. 1–8). Berlin: Springer.

Weickert, J., & Brox, T. (2002). Diffusion and regularization of vector- and matrix-valued images. In M. Z. Nashed & O. Scherzer (Eds.), *Contemporary mathematics: Vol. 313. Inverse problems, image analysis, and medical imaging* (pp. 251–268). Providence: AMS.

Weickert, J., & Hagen, H. (Eds.) (2006). *Visualization and processing of tensor fields*. Berlin: Springer.